Green fabrication of fully bio-based poly(vinyl alcohol)/phytic acid composite aerogels with robust 3D networks for sustainable thermal insulation and fire safety

Suliang Gao,[a,b] Siqi Huo,[*,c,d] Ruiping Wang,[b] Miaojun Xu,[*,a,b] Sheng Li,[a,b] Bin Li[*,a,b]

[a] *Key Laboratory of Bio-based Material Science and Technology of Ministry of Education, Northeast Forestry University, Hexing Road 26, Harbin, 150040, China*

[b] *Heilongjiang Key Laboratory of Molecular Design and Preparation of Flame Retarded Materials, College of Chemistry, Chemical Engineering and Resource Utilization, Northeast Forestry University, Harbin, 150040, China*

[c] *Centre for Future Materials, University of Southern Queensland, Springfield Central, QLD 4300, Australia*

[d] *School of Engineering, University of Southern Queensland, Springfield 4300, Australia*

* Corresponding Author:

E-mail addresses: Siqi.Huo@unisq.edu.au (S. Huo), xumiaojun@nefu.edu.cn (M. Xu), libinzh62@163.com (B. Li)

Abstract: The development of sustainable thermal insulation materials that combine light weight, high strength, and fire retardancy is essential to support global carbon neutrality goals. Herein, fully bio-based polyvinyl alcohol/phytic acid (PVA/PA) composite aerogels were fabricated through an environmentally benign refrigerator-assisted freezing process without the use of toxic solvents. The strong reactivity of bio-

based phytic acid enabled the formation of a robust micro–nano three-dimensional (3D) network, yielding an aerogel with low density (0.075 g cm^{-3}), high porosity (94.21%), and ultralow thermal conductivity (33.6 $mW \cdot m^{-1} \cdot K^{-1}$). Benefiting from its micro-nano 3D nework, the aerogel exhibited excellent mechanical robustness, with compressive strength and specific modulus increasing by 225.7% and 294.5%, respectively. Due to the formation of intrinsic intumescent flame retardant (IFR) system, the aerogel achieved an extremely high limiting oxygen index (LOI) of 41.9% and a UL 94 V–0 rating (self–extinguishing time of only 1.8 s) with significantly reduced heat and smoke release during combustion. Furthermore, a solvent–free thermal chemical vapor deposition (CVD) treatment imparted durable hydrophobicity (water contact angle = 145.6º). This work provides a green and scalable strategy for producing multifunctional bio-based aerogels with great potential for high–performance and sustainable thermal insulation applications.

Keywords: Bio–based polyvinyl alcohol; Phytic acid; Composite Aerogel; Thermal insulation; Fire safety

1. Introduction

The global energy crisis and environmental pollution have become two of the most pressing challenges today, with profound implications for sustainable development, economic stability, and public health [1]. In this context, green thermal insulators have become indispensable for enhancing energy efficiency and mitigating excessive energy

consumption [2]. Among these, bio–based aerogels have attracted considerable attention as promising thermal insulators owing to their ultralow thermal conductivity, environmental friendliness, and inherent biocompatibility [3-5].

PVA is an economical, non–toxic, and biodegradable polymer [6-8]. PVA–based aerogels typical exhibit superior mechanical toughness and thermal stability compared with those derived from other bio–based materials such as cellulose nanofibrils (CNF) [9], ammonium alginate (AL) [10], and chitosan (CS) [11]. Moreover, PVA can be synthesized not only frompetroleum–based feedstocks but also renewable biomass[12]. Thus, the production of bio–based PVA aerogels has the potential to reduce reliance on fossil resources [13]. However, the inherent flammability of PVA significantly limits its broader application potential [14,15].

Flame retardants (FRs) are frequently added to the PVA matrix to improve its flame retardancy. Among these, phosphorus–based FRs demonstrate higher efficiency than inorganic FRs and are more environmentally friendly than halogen–based FRs [16-18]. However, most phosphorus–based FRs are derived from non–renewable minerals, raising concerns about resource depletion[19,20]. Phytic acid (PA) is a naturally present organic acid abundant in rice bran, nuts, and grains, of which the phosphorus content reaches 28 wt% [21]. Its non–toxic nature and high phosphorus content make it a highly promising green and efficient FR [22]. Cao et al. [23] reported that the polysaccharides (AL)–based AL5PA0.5 aerogel with only 9 wt% of PA achieved a UL94 V–0 rating and an LOI of 38.0%, while maintaining a high specific modulus of 83.1 $MPa \cdot cm^3 \cdot g^{-1}$. Wang et al. [24] highlighted that the proteins (PG) –

based PG5PA1 aerogel with 16.7 wt% of PA exhibited significantly enhanced flame retardancy and mechanical strength. The improved flame retardancy was attributed to the formation of an intrinsic IFR system, in which AL or PG served as 'carbon' and 'gas' sources, while PA acted as the 'acid' source. Moreover, PA acted as a crosslinking agent, forming stable interaction with AL or PG to enhance mechanical strength [25].

Although PA had been applied in the fabrication of flame–retardant PVA–based aerogels, the resultant aerogels still suffered from poor flame retardancy [26-28]. Moreover, conventional pre–freezing media, such as liquid nitrogen (–196.0℃) and solid carbon dioxide/ethanol baths (–70.0℃), often induces cracking in the aerogel due to extremely low temperatures and releases greenhouse gases [29]. In contrast, pre–freezing in a refrigerator (–20.0℃) offers advantages, including simplicity, cost–effectiveness, and safety, making it a promising alternative. However, the relatively slow freezing rate at this temperature can result in larger pore diameters and structural defects. Previous research has demonstrated that cyclic freezing and thawing can effectively migrate this issue [8]. To date, few studies have reported the fabrication of green composite aerogels using bio–based PVA and PA via a refrigerator–assisted freezing process.

In this study, an intrinsically IFR bio–based composite aerogel was successfully prepared by refrigerator–assisted freezing and chemical vapor deposition (CVD) using polymethylhydrosiloxane (PMHS). The fire retardancy, thermal insulation, mechanical properties and hydrophobicity of the resulting PVA/PA aerogel were investigated in detail. The flame-retardant mechanism was also studied.

2. Experimental

2.1. Materials

Bio–based polyvinyl alcohol (PVA–1799) was provided by Wanwei Biomass Technology Co., Ltd. (Hechi, China). Phytic acid (PA) aqueous solution of 50 wt% was obtained from Sinopharm Chemical Reagent Co., Ltd. (Shanghai, China). Polymethylhydrosiloxane (PMHS) was purchased from Aladdin Scientific Co., Ltd. (Shanghai, China).

2.2. Fabrication of Bio-Based PVA/PA Composite Aerogels

As illustrated in Fig.1a, bio–based PVA/PA composite aerogels were prepared by the water–assisted fabrication. Firstly, the process began by dissolving 6 g of bio–based PVA in 94 mL of deionized water at 85℃ for 2 h, resulting in a 6 wt% PVA aqueous solution. The solution was then allowed to cool down to a temperature rangeof 40–50℃. Meanwhile, 12g of PA aqueous solution was mixed with 88 mL of deionized water and then stirred magnetically at 40 °C for 30 min to produce a 6 wt % PA solution. Based on the desired 85/15 mass ratio of PVA to PA, 15 mL of 6wt% PA solution was added dropwise in five portions to 85 mL of the 6 wt % PVA solution. Following each addition, the mixture solution was subjected to high–speed shear mixing at 2000 rpm for 5 min to achieve homogeneous dispersion and avoid localized excessive concentration. Secondly, the mixture was poured into mold and subsequently frozen in a refrigerator for 8 h, after which it was allowed to thaw at room temperature for another 8 h. This freeze–thaw process was repeated for a total of three cycles. Finally, PVA85/PA15 composite aerogel was obtained after under vacuum conditions at –80℃

for a duration of 72 h using a SCIENTZ–18N freeze–drying system (manufactured in Ningbo, China). Other specimens, including PVA95/PA5, PVA90/PA10, PVA80/PA20, and pure PVA aerogel, were fabricated using the identical preparation method.

2.3. Hydrophobic Aerogels Preparation

PMHS was introduced to enhance the hydrophilicity of sample through a CVD process. In detail, 1 mL of PMHS were introduced into a desiccator containing the PVA85/PA15 aerogel. The desiccator was sealed and kept at 80 ℃ in a hot–air oven for 24 h to promote the salinization reaction. Following, the aerogel was placed in a fume hood for 8 h to eliminate any residual silane. The final hydrophobic aerogel sample was labelled as PMHS–PVA85/PA15.

2.4. Characterizations

The microstructure and elemental composition of the aerogel and carbon layer were examined using a JSM‑7500F scanning electron microscope (JEOL, Japan) equipped with an energy dispersive X‑ray spectrometer (EDS). Fourier transform infrared spectroscopy (FT‑IR) analysis was carried out using a Nicolet IS10 instrument (Thermo Scientific, USA) over a wavelength range of 400 to 4000 cm^{-1}. X–ray photoelectron spectroscopy (XPS) was employed to analyse high-resolution spectra of the C1s, P2p, and Si2p regions, utilizing a K‑Alpha X‑ray photoelectron spectrometer (Thermo Scientific, USA). Nitrogen adsorption‑desorption isotherms were recorded at 77 K using a Belsorp‑Max device (BEL, Japan). The bulk density (ρb) was calculated by dividing the sample's mass by its volume, while the porosity

was derived using Equation (1).

$$porosity = (1 - \frac{\rho_b}{w_{PVA} \times \rho_{PVA} + w_{PA} \times \rho_{PA}}) \times 100\% \quad (1)$$

WPVA and WPA denote the respective proportions of PVA and PA. The densities were supplied by the manufacturer, with PVA having a density of 1.27 g·cm^{-3} and PA a density of 1.43 g·cm^{-3}. The mechanical properties of the aerogels were evaluated using an RGM-6005 testing machine (Shenzhen, China) at a compression speed of 2mm·min^{-1}. AC–Therm TCi analyser (Fredericton, Canada) was employed for thermal conductivity measurements, according the ASTM D7984 standard. A TESTO–869 thermal camera (TESTO, Germany) was employed to capture infrared thermal images of the samples placed on a hot stage (70℃) and a cold stage (–20 ℃). The sample specimens were with a diameter measuring 45 mm and a height of 15 mm. To evaluate flame retardancy, CZF–5 vertical combustion and JF-3 oxygen index meter (Jiangning, China) was used, following the UL94 and GB/T 2046.2–2009standards, respectively. The samples for the UL94 test had a diameter of 15 mm and a height of 100 mm, while the specimens used in the LOI test were 120 mm long, 10 mm wide, and 10 mm thick. Thermal degradation behaviors were analyzed using a TGA–Q5000 (PerkinElmer, USA) under a nitrogen environment, with a heating rate of 10℃·min^{-1}. Cone calorimetry experiments were performed using a VOUCH–6810 cone calorimeter (VOUCH, China) under a thermal flux of 35 kW·m^{-2}, using with the specimen had a length of 100 mm, a width of 100 mm, and a thickness of 4 mm. A TGA–8000 system integrated with an FT–IR spectrometer (PerkinElmer, USA) was used under nitrogen

atmosphere to analysis TG–FT–IR, at a heating speed of 20℃·min^{-1}. The water contact angle (WCA) was measured using a DSA100S instrument (Kruss, Germany).

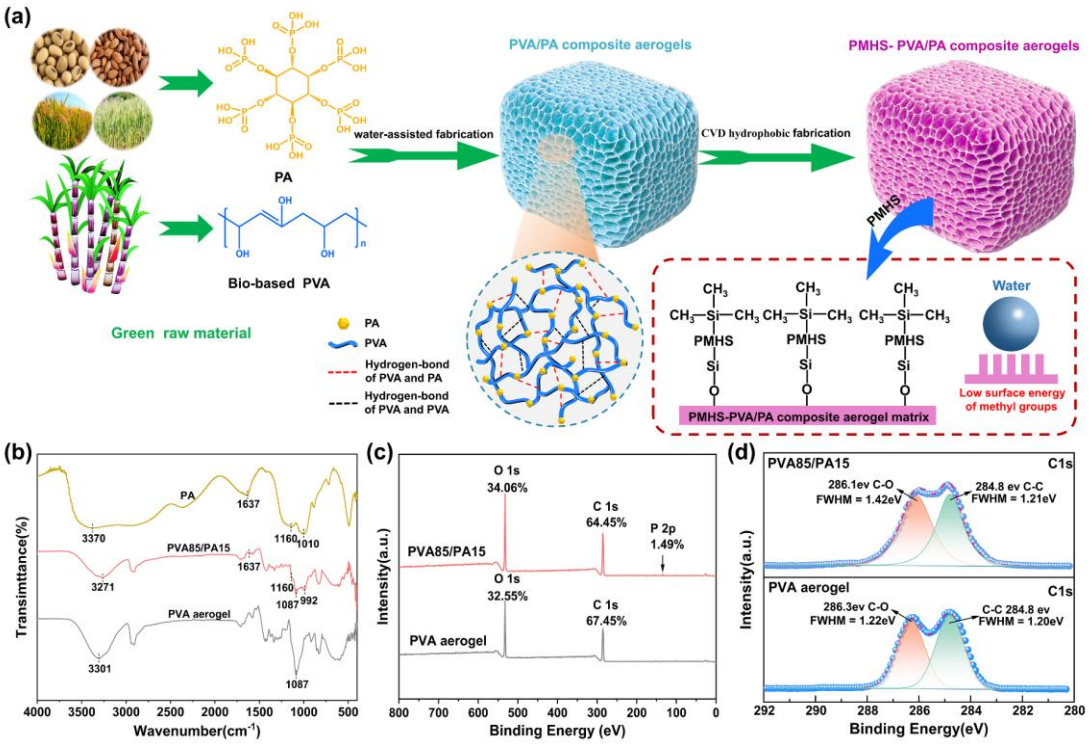

Fig. 1. (a) Fabrication procedure and interface interaction of PVA/PA composite aerogels. (b) FT–IR spectra. (c) XPS curves. (D) High–resolution C 1s spectra.

3. Results and Discussion

3.1. Microstructures Analysis

Green PVA/PA composite aerogels were fabricated using water as solvent via refrigerator–assisted freezing. The chemical structure of these aerogels was first investigated by FT–IR. As illustrated in Fig.1b, PA exhibited distinct absorption peaks at 3370, 1638, 1160, and 1010 cm^{-1}, corresponding to the –OH stretching vibration, asymmetric O–P–O stretching vibration, P=O stretching vibration, and P–O stretching vibration, respectively[30-33] .For pure PVA aerogel, the –OH and C–O stretching vibration peak appeared at 3301 and 1087 cm^{-1}, respectively [34].Compared with pure

PVA aerogel, the –OH stretching vibration peak in PVA85/PA15 composite aerogel shifted to 3271 cm^{-1}, while the P–O stretching vibration peak shifted from 1010 to 992 cm^{-1} and divided into multiple smaller, less intense sub-peaks. These alterations in the spectrum were ascribed to the robust hydrogen bonding interactions occurring between the hydroxyl (–OH) groups in PVA and the phosphoric acid (P–OH) groups in PA, resulting in a redshift of the –OH and P–O stretching vibrations. Meanwhile, certain P–OH groups still retain their original vibrational frequencies, as they either do not form hydrogen bonds or form only weak hydrogen bonds with–OH groups. The coexistence of P–O groups with different vibrational frequencies led to the splitting of the original broad absorption peak into several distinct sub–peaks.

XPS results (Fig.1c–d) revealed the presence of the P element in the PVA85/PA15 composite aerogel. Furthermore, in the high-resolution C 1s spectrum of the PVA85/PA15 composite aerogel, the C–O peak was moved to a lower binding energy level of 286.1 eV, accompanied by an increase in the full width at half maximum (FWHM) to 1.42 eV. This was because the hydrogen bonds induced a redistribution of the electron cloud density toward the oxygen atoms, thereby increasing the electron density near the α-C atoms within the C–O bonds and leading to a decrease in the binding energy of the C–O peak [35]. Furthermore, the dynamic and randomly distributed nature of hydrogen bonds created a more diverse chemical environment around the

α–C atoms in C–O bonds, which contributed to the increased FWHM [36]. The above results indicated that the PVA/PA composite aerogels were successfully prepared through the strong hydrogen–bonding interactions between PVA and PA.

The morphology structure of aerogel samples was examined through SEM [37]. The pure PVA aerogel exhibited an irregular micro–nano network structure with relatively large micro–scale pores (Fig. 2a). This result can be ascribed to the slow and random growth of ice crystals during the refrigerator–assisted freezing process, which was further influenced by the inherently weak intermolecular interactions between PVA chains. However, compared with our previous study [13], the pure PVA aerogel showed a significantly reduced number of weak intermolecular connections due to the freeze-thaw cycling process. This structural improvement was presumably associated with the dynamic reconstruction of hydrogen bond between PVA molecules induced by the freeze–thaw cycles, thereby promoting the self–healing of internal structural defects [38,39]. As illustrated in Fig.2b–e, the composite aerogels demonstrated a notable decrease in micropore size due to the introduction of PA, leading to the formation of a more compact microstructure. Notably, PVA85/PA15 composite aerogel demonstrated a more regular micro–nano network structure and a significantly smaller micropore size compared to the pure PVA aerogel. These alterations in structure were mainly due to the strong chelation ability and high reactivity of PA, which introduced additional cross–linking sites and formed stable interactions with PVA. The resultant stable cross–linking network can effectively inhibit excessive ice crystal growth, thereby reducing the micro–pore size. Meanwhile, it also functioned as a robust supporting skeletal,

enhancing the stability of pore walls and decreasing disordered interconnections of the composite aerogel. However, PVA80/PA20 composite aerogel exhibited evident structural damage, which may result from excessive PA leading to over-crosslinking and agglomeration effects. Furthermore, EDS element mapping results demonstrated that the distribution patterns of C, O, and P elements was uniform within the PVA85/PA15 composite aerogel, indicating superior compatibility between PA and PVA (Fig. 2f).

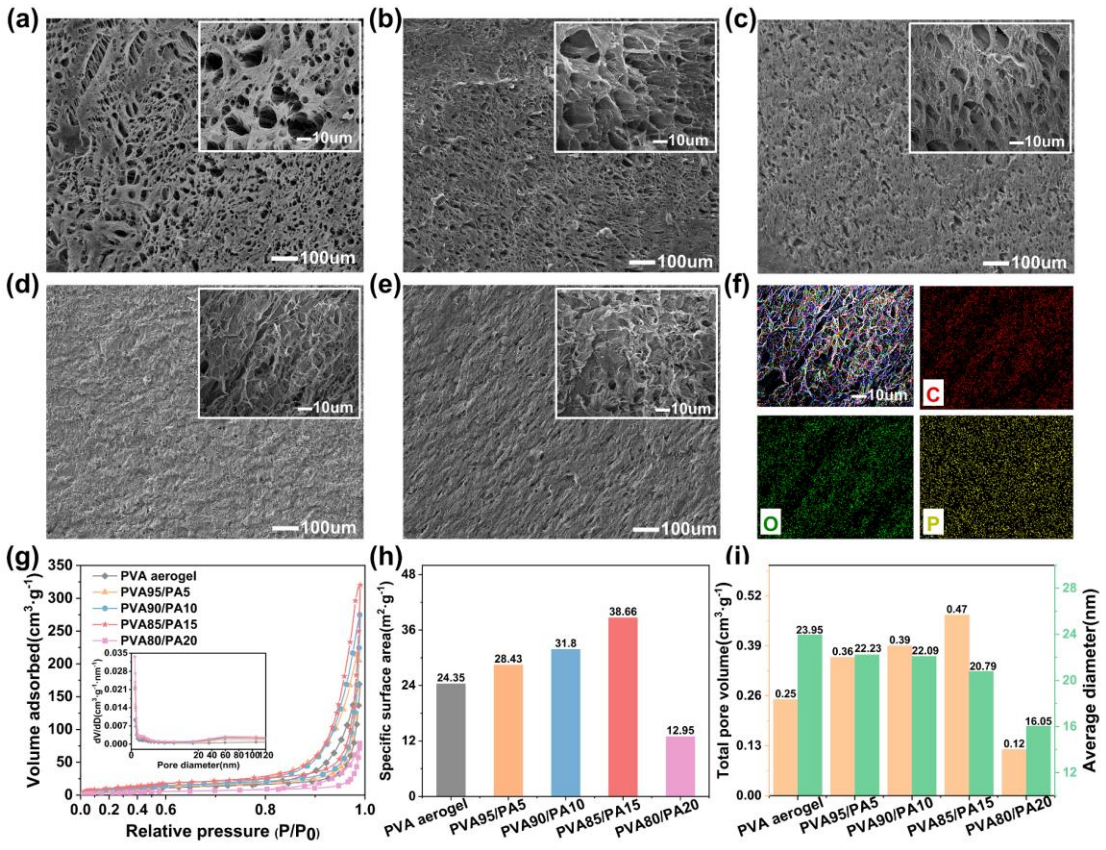

Fig. 2. SEM micrographs of the aerogels: (a) PVA; (b) PVA95/PA5; (c) PVA90/PA10; (d) PVA85/PA15; and (e) PVA80/PA20. (f) EDS mapping of the PVA85/PA15 composite aerogel. (g) Nitrogen adsorption–desorption isotherms along with pore size

distribution. (h) Specific surface area analysis. (i) Total pore volume and average pore diameter.

The nanoscale pore structure of these aerogels was analyzed using nitrogen adsorption–desorption isotherms, applying the Brunauer–Emmett–Teller (BET) and Barrett–Joyner–Halenda (BJH) methods [40,41]. As illustrated in Fig.2g, all aerogel sample displayed a type IV isotherm featuring an H3–type hysteresis loop. The size distribution of nanoscale pores was mainly characterized by mesopores measuring between 2 and 50 nm, accompanied by a smaller proportion of micropores (less than 2 nm) and macropores (exceeding 50 nm). As shown in Fig.2h–i, the specific surface area and total pore volume of the composite aerogels first increased and then decreased with the rising PA content, whereas the average pore size consistently reduced. Among the evaluated materials, the PVA85/PA15 composite aerogel demonstrated the largest specific surface area (SSA) of 38.66 $m^2 \cdot g^{-1}$, coupled with a peak total pore volume of 0.47 $cm^3 \cdot g^{-1}$, while maintaining a comparatively small average pore size of 20.79 nm. These results can be attributed to PA acting as crosslinking agents, offering abundant crosslinking sites. The intense interaction between PVA and PA facilitated the formation of additional nanopores within the aerogel structure. However, PVA80/PA20 composite aerogel exhibited a notable decrease in SSA, total pore volume, and average pore size decreasing to 12.95 $m^2 \cdot g^{-1}$, 0.12 $cm^3 \cdot g^{-1}$, and 16.05 nm, respectively. This decline was attributed to an excessive PA content, which may induce over–crosslinking, thereby limiting the mobility of PVA chains, reducing pore sizes, and

potentially impairing the integrity and connectivity of the nanoporous network. These findings align with the SEM observations.

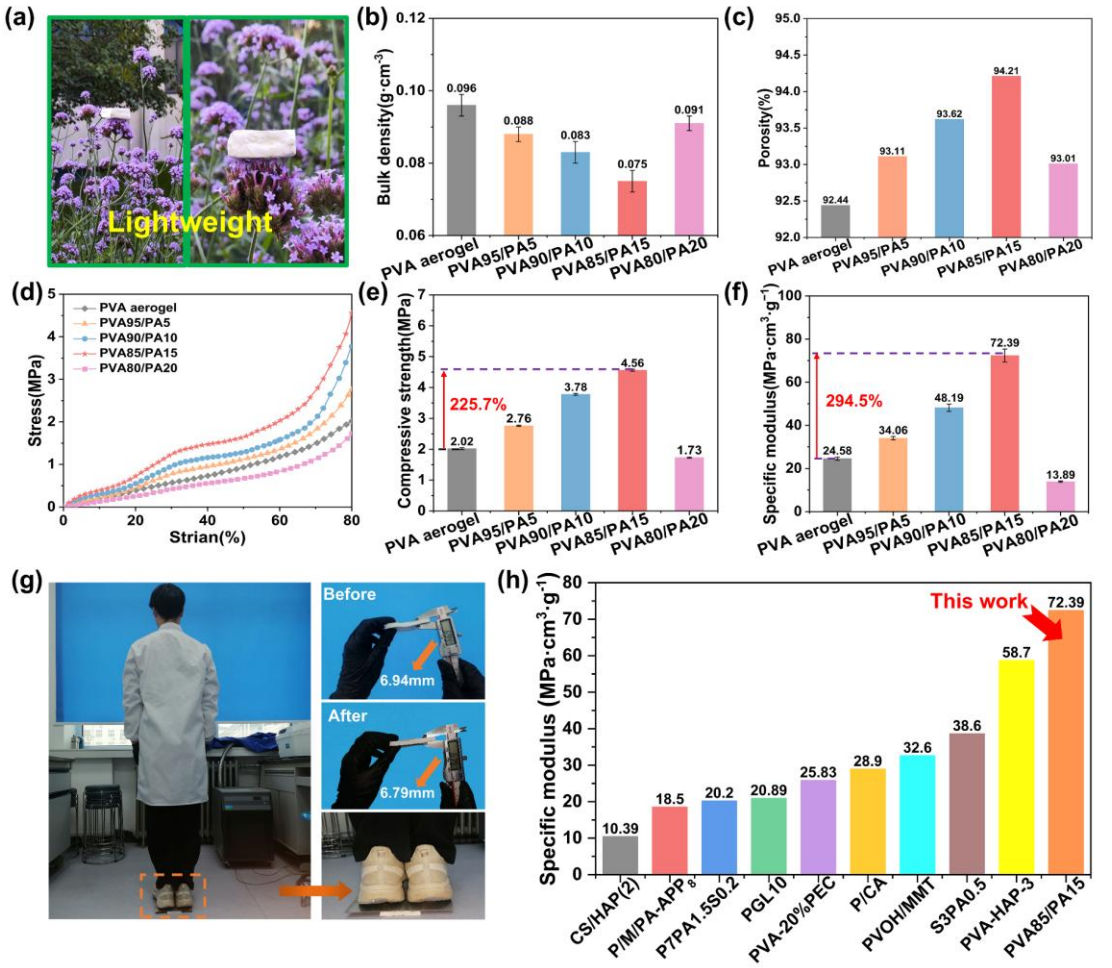

Fig. 3. (a) Digital photo of PVA85/PA15 composite aerogel stabilized on a dandelion; (b) Bulk density. (c) Porosity. (d) Stress versus strain curves. (e) Compressive strength when the strain reaches 80%. (f) Sample–specific modulus. (g) The photograph illustrated that the weight of a 65 kg adult supported by PVA85/PA15 composite aerogel. (h) The contrast column diagram of specific modulus for PVA85/PA15 composite aerogel and other aerogels.

3.2. Physical and Mechanical Properties

As shown in Fig.3a–c, the composite aerogels exhibited an initially decreased and subsequently increased in the bulk density with increasing PA content, while the porosity displayed the opposite trend. PVA85/PA15 composite aerogel showed the minimum bulk density (0.075 $g \cdot cm^{-3}$) and the maximum porosity (94.21%). Moreover, the aerogel could be stably placed on a flower, showing its exceptional lightweight nature. These findings may be explained by the development of a strong three-dimensional network framework, which raised from the strong intermolecular bonds formed between PVA and PA. This robust network effectively resisted expansion pressure during pre–freezing and capillary tension during freeze–drying, reducing the shrinkage of aerogel. However, PVA80/PA20 composite aerogel exhibited an increased bulk density (0.091 $g \cdot cm^{-3}$) and reduced porosity (93.01%) with further increase in PA content. These results were attributed to the excessive PA content, which promoted self–agglomeration and over–crosslinking, thus altering the aerogel's porous framework and resulting in the increased density alongside the reduced porosity.

The uniaxial compression test was conducted to assess the mechanical properties of composite aerogels [42]. As illustrated in the stress–strain diagrams (Fig. 3d), all aerogel specimens displayed a linear elastic behavior within the strain range of 0% to 5%, and the stress enhanced progressively as the strain increased in the strain region of 5% to 80%, which can be explained by the structural densification occurring within the aerogel specimens. Among the evaluated specimens, the PVA85/PA15 composite aerogel exhibited the maximum compressive strength, reaching 4.56 MPa at 80% strain,

along with the highest specific modulus of 72.39 MPa·cm³·g⁻¹. Compared with pure PVA aerogel, the compressive strength and specific modulus of the aerogel increased by 225.7% and 294.5%, respectively, indicating a significant improvement in compressive performance (Fig.3e–f). Even under the load of a 65 kg adult, a mere 7.2 g of the aerogel exhibited only 0.15 mm of deformation, further confirming its excellent structural stability and load–bearing capacity (Fig.3g). Moreover, as shown in Fig. 3h, the specific modulus of the composite aerogel was much higher than those of most PVA–based aerogels and bio–based aerogels [15-17,27,43-47]. Additionally, the aerogel was fabricated through a simple refrigerator-assisted freezing process. Thus, the PVA85/PA15 composite aerogel featured obvious advantages in both mechanical performance and fabrication simplicity.

The enhancements in mechanical properties can be ascribed to the following critical factors. Firstly, the manufacturing process played a crucial role for these improvements. The combination of batch feeding of PA with high–speed shearing significantly enhanced its dispersion in the PVA aqueous solution, effectively suppressing its self–aggregation behavior. The freeze–thaw cycling process facilitated the reconstruction of the dynamic hydrogen bond network, which helped eliminate internal structural defects and provided structural support for the high compressive performance of composite aerogels [48]. Secondly, PA molecules containing eight phosphate groups exhibited strong chelating capacity and high reactivity, enabling them to form hydrogen bonds with PVA, thereby acting as a ‘molecular bridge’. These hydrogen bonds can enhance the 3D network structural strength of the aerogel. The

robust macro–nano 3D network structure formed within the PVA85/PA15 composite aerogel provided multiple stress dispersion pathways due to the addition of a suitable amount of PA, effectively mitigating stress concentration [49]. However, excessive PA could cause self-aggregation and over–crosslinking, causing damage to the structure of the PVA80/PA20 aerogel, resulting in increased brittleness and a considerable decrease in compressive strength.

3.3. Thermal Insulation

The thermal insulation capability of aerogel samples was assessed through the measurement of their thermal conductivity [50]. The thermal conductivity of pure PVA aerogel was measured at 40.6 $mW \cdot m^{-1} \cdot K^{-1}$. As the PA content increased, the thermal conductivity of the composite aerogels initially decreased and subsequently increased. It is worth noting that the PVA85/PA15 composite aerogel exhibited the minimum thermal conductivity at 33.6 $mW \cdot m^{-1} \cdot K^{-1}$, while the PVA82/PA20 composite aerogel demonstrated the maximum thermal conductivity of 42.7 $mW \cdot m^{-1} \cdot K^{-1}$ (Fig. 4a).

To more accurately reflect real–world application scenarios, pure PVA aerogel and PVA85/PA15 composite aerogel were evaluated under controlled temperature conditions using a cold stage set at –20℃and a hot stage at 70℃ (Fig. 4b). Following a 15min exposure to the cold stage, the top surface temperature of pure PVA aerogel dropped significantly to 9.8℃, whereas that of PVA85/PA15 composite aerogel remained relatively higher at 11.2℃. After the same time at the hot stage, the upper surface temperature of pure PVA aerogel rose significantly to 42.2℃, while PVA85/PA15 composite aerogel demonstrated the lower temperature of 38.1℃

(Fig.4c). The findings indicated that the PVA85/PA15 composite aerogel possessed excellent thermal insulation capabilities. The aerogel offered a feasible solution for energy–saving in building applications by maintaining warmth in winter and coolness in summer (Fig.4d).

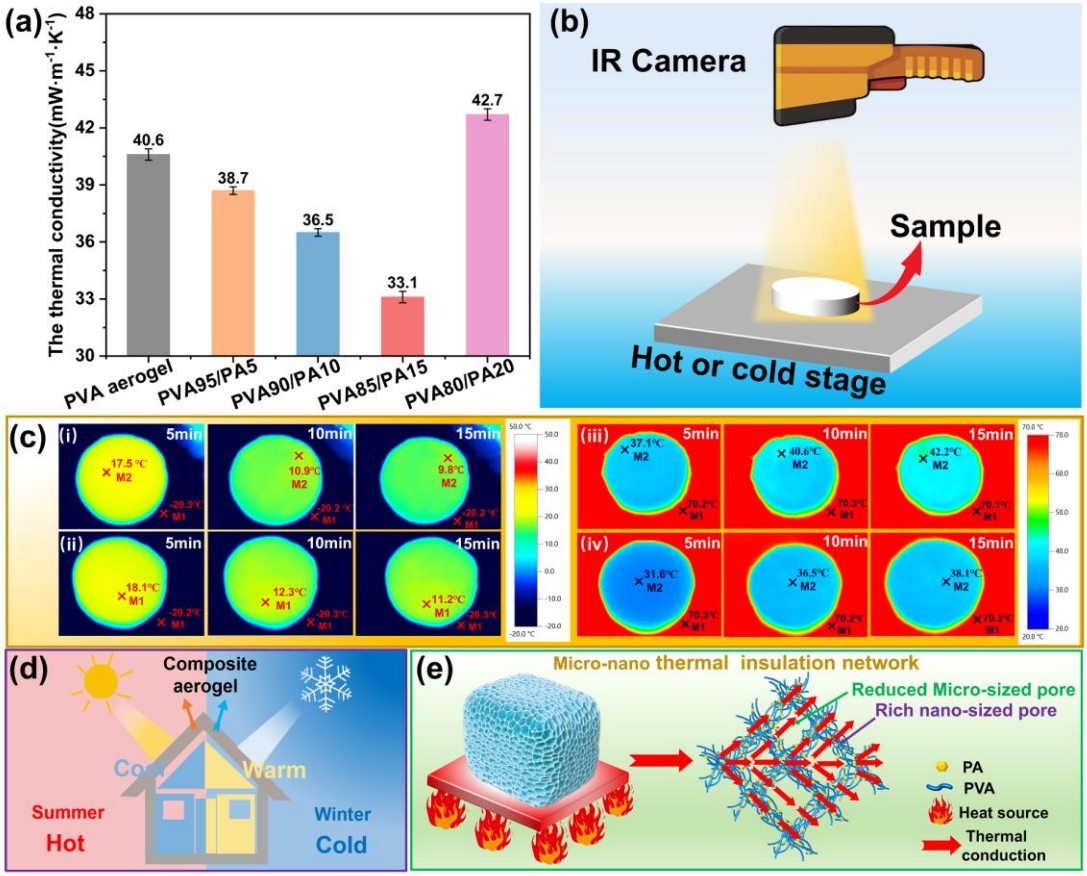

Fig.4 (a) Thermal conductivity results. (b) Simulation setup of the visual thermal insulation testing apparatus. Top–view thermal images of the PVA aerogel and the PVA85/PA15 composite aerogel (1.5 cm height) after being placed on (c) a cold stage (–20℃) and (d) a heated stage (70℃) for 15 min. (e) Potential application of these composite aerogels in the construction industry. (f) Illustration of the thermal insulation mechanism within the composite aerogels.

Additionally, the heat insulation principle of composite aerogels was analyzed. The overall thermal conductivity (λ_t) was primarily influenced by three factors: thermal radiation (λ_{rad}), thermal convection (λ_{conv}), and thermal conduction (λ_{cond}). Among these, λ_{cond} comprised both solid thermal conduction (λ^s_{cond}) and gas thermal conduction (λ^g_{cond}). The values of λ_{rad} and λ_{conv} were typically insignificant in porous materials featuring pore diameters less than 1 mm under normal temperature conditions [51]. As a result, λ^s_{cond} and λ^g_{cond} determined the effective thermal conductivity (λ_e), as described in Equations (2–4).

$$\lambda_t = \lambda_{rad} + \lambda_{conv} + \lambda_{cond} \quad (2)$$

$$\lambda_{cond} = \lambda^s_{cond} + \lambda^g_{cond} \quad (3)$$

$$\lambda_e = \lambda^s_{cond} + \lambda^g_{cond} \quad (4)$$

$$\lambda^s_{cond} = \lambda_0 \frac{\rho_b}{\rho_s} \frac{v}{v_s} \quad (5)$$

$$\lambda^g_{cond} = \frac{\lambda_{g0} \Pi}{1+2\beta k_n} \quad (6)$$

$$k_n = \frac{l}{D} \quad (7)$$

λ^s_{cond} is given by Equation (5), where λ_o is the material's intrinsic thermal conductivity; ρ_b and ρ_s represent the bulk density and the skeletal density, respectively; ν and νs are the phonon propagation and vibrational velocities [52]. λ^g_{cond} is described by Equation (6), where λ_g. represents the thermal conductivity of air in free space (24 $mW \cdot m^{-1} \cdot K^{-1}$); Π denotes porosity; ß denotes air coefficient; and k_n stands for Knudsen number. According to Equation (7), l is the mean free path of air molecules (approximately 70 nm), and d is the average pore diameter of aerogel [53].

For λ^{s}_{cond}, the minimum ρ_b of 0.075 g·cm^{-3} in PVA85/PA15 composite aerogel was exhibited among all the aerogel samples. Meanwhile, the incorporation of an appropriate amount of PA facilitated the formation of a more complex and tortuous micro–nano 3D network within the composite aerogel, which effectively elongated and scattered phonon propagation paths. These factors collectively contributed to a significant reduction in λ^{s}_{cond}. For λ^{g}_{cond}, the composite aerogel displayed notably smaller micro–pore and nano–pore diameters, and it's the average nano–pore diameter (20.79 nm) was much smaller than the mean free path of air molecules (70 nm). This well–developed nanoscale network effectively restricted air molecule movement as a barrier due to its highest total nano-pore volume (0.47 cm^3·g^{-1}), thereby enhancing Knudsen effect and significantly reducing λ^{g}_{cond}. Consequently, PVA85/PA15 composite aerogel achieved the lowest λ_e (Fig. 4e).

3.4. Flame Retardancy and Thermal Stability

The flame–resistant properties of the aerogel specimens were assessed through UL94 and LOI testing approaches [54]. As illustrated in Fig.5a and presented in Table S1, pure PVA aerogel ignited rapidly and produced molten drips that easily set fire to the underlying cotton fabric. Consequently, it did not meet the UL94 standard and showed a relatively low LOI of merely 18.6%. In contrast, PVA95/PA5 composite achieved a UL94 V–0 rating and exhibited a significantly enhanced LOI value reaching 28.5% through adding only 5 wt% PA, and the PVA85/PA15 composite aerogel, possessing optimal mechanical strength and thermal insulation, achieved a notably short self-extinguishing time of only 1.8 s in the UL94 test (Fig.5b) with an LOI value

of 41.9%. Moreover, compared with most PVA–based composite aerogels with the UL94 V–0 rating [16,18,26,43,50,55-57], our PVA85/PA15 aerogel demonstrated much higher LOI value (Fig.5c). Although the PVA80/PA20 composite demonstrated the most effective flame–retardant performance, its use in practical applications was constrained by its inferior mechanical and thermal insulation. The experimental results mentioned above are primarily due to two key factors: (i) the evenly dispersion of PA within the PVA matrix; and (ii) the intrinsic IFR system, in which PVA served as the primary "carbon source" and secondary "gas source", while PA acted as the "acid source". As a result, the composite aerogel exhibited excellent flame-retardant performance.

The combustion characteristics of PVA/PA aerogels were assessed through cone calorimetry test (CCT) [58]. As illustrated in Fig.5d–j and Table S2, pure PVA aerogel demonstrated a high degree of flammability, characterized by a short time to ignition (TTI) of merely 10 s. In contrast, the TTI of the PVA85/PA15 composite aerogel rose to 34 s, with an enhancement of 340%. This extended TTI provided valuable time for initial evacuation and fire response. Moreover, PVA85/PA15 showed an 84.5% reduction in peak heat release rate (pHRR) and an 81.1% decrease in total heat release (THR) relative to pure PVA aerogel, thereby significantly reducing the risk of thermal runaway during fire incidents. Additionally, its peak smoke production rate (pSPR), total smoke production (TSP), and peak carbon monoxide production rate (pCOP) were reduced by 55.6%, 61.8%, and 69.4%, respectively, effectively lowering the risk of smoke-induced asphyxiation during fires. More significantly, there was an 89.9%

reduction in the Fire Growth Rate Index (FIGRA), demonstrating outstanding fire safety capabilities. Therefore, the PVA85/PA15 composite aerogel demonstrated considerable promise in thermal insulation applications, owing to its minimal fire risk.

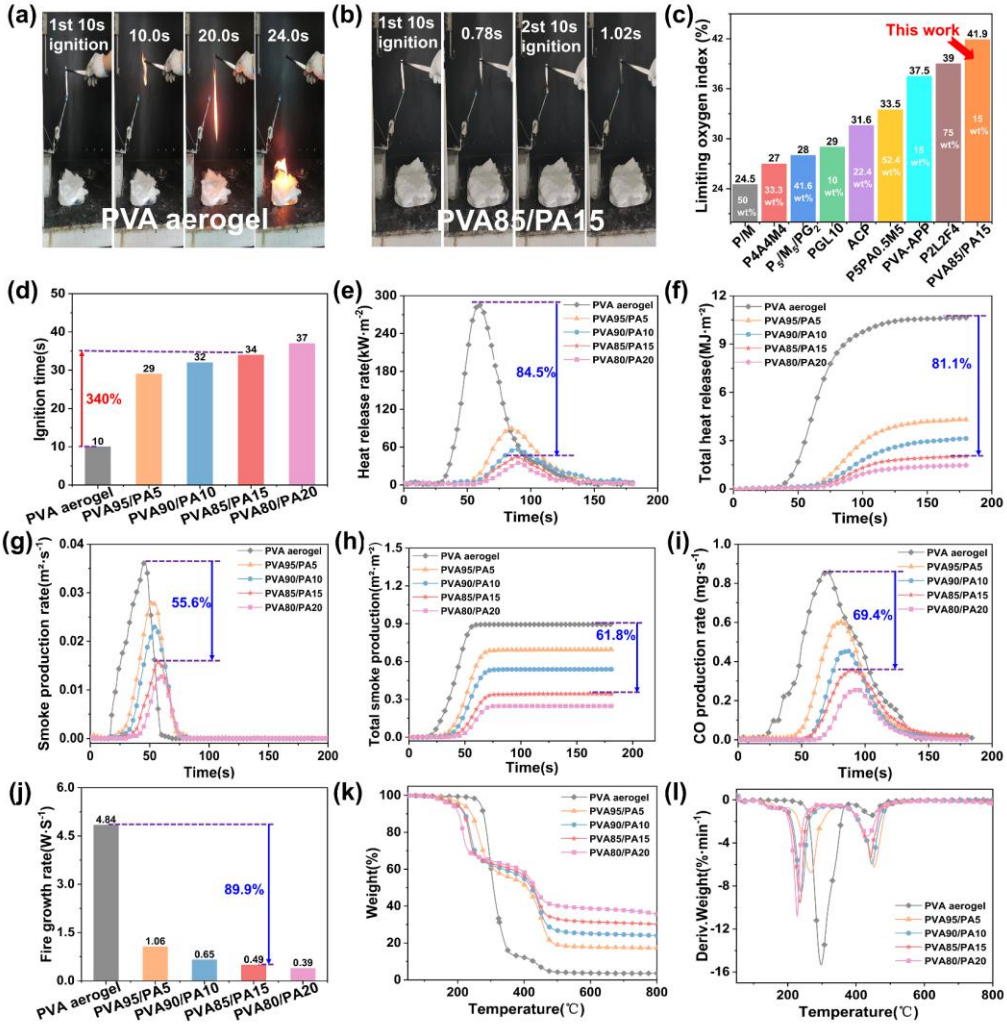

Fig. 5. Digital images of the UL94 test: (a) PVA aerogel and (b) PVA85/PA15.

(c) The contrast column diagram of flame-retardant properties for PVA85/PA15 composite aerogel and other PVA–based composite aerogels with UL94V–0 rating. Cone test:(d) Ignition time; (e) HRR curves; (f) THR curves; (g) SPR curves; (h) TSP curves; (i) COP curves; and (j) FIGRA. (k) TGA curves. (l) DTG curves.

The thermal stability of the aerogel samples was also investigated, with the corresponding curves and data displayed in Fig.5k–l and Table S3. Compared to pure PVA aerogel, the initial thermal degradation temperature ($T_{5wt\%}$), as well as the temperature corresponding to the first maximum weight loss peak (T_{1peak}) of the composite aerogels were significantly decreased. Additionally, the temperature corresponding to 50% mass loss ($T_{50wt\%}$) and the residual char yield measured at 800°C both showed gradual increases. For the PVA85/PA15 composite aerogel, its $T_{5wt\%}$ and T_{1peak} decreased to 195.1℃ and 235.7℃, respectively, while its $T_{50wt\%}$ increased to 427.4℃. Moreover, the residual char yield at 800℃ of the PVA85/PA15 composite aerogel significantly enhanced to 30.2wt%. The outcomes may be attributed to the catalytic carbonization effect of PA under heating [59,60]. The formed char layer is capable of not only efficiently limiting the diffusion of heat and oxygen but also suppressing the volatilization of PVA decomposition products, which in turn improves the thermal stability of the composite aerogel.

3.5. Flame Retardant Mechanism

The flame–retardant mechanism of PVA85/PA15 composite aerogel was analyzed. As observed in Fig.6a, a minimal quantity of char residue was present for pure PVA aerogel, while numerous irregular big pores were showed in the char surface after CCT. This relatively loose char layer exhibited limited effectiveness in preventing heat and oxygen from penetrating into the interior of the matrix. Furthermore, the big porous structure failed to prevent the release of significant quantities of flammable volatile substances from the matrix, which subsequently acted as additional fuel,

promoting flame propagation and accelerating the overall combustion process. In contrast, a more continuous, uniform, and dense char layer with a lot of closed bubbles was formed after the combustion of PVA85/PA15 composite aerogel. This compact char layer can effectively hinder the transfer of heat and oxygen, while substantially suppressing the release of flammable volatiles, thus greatly improving the flame retardancy.

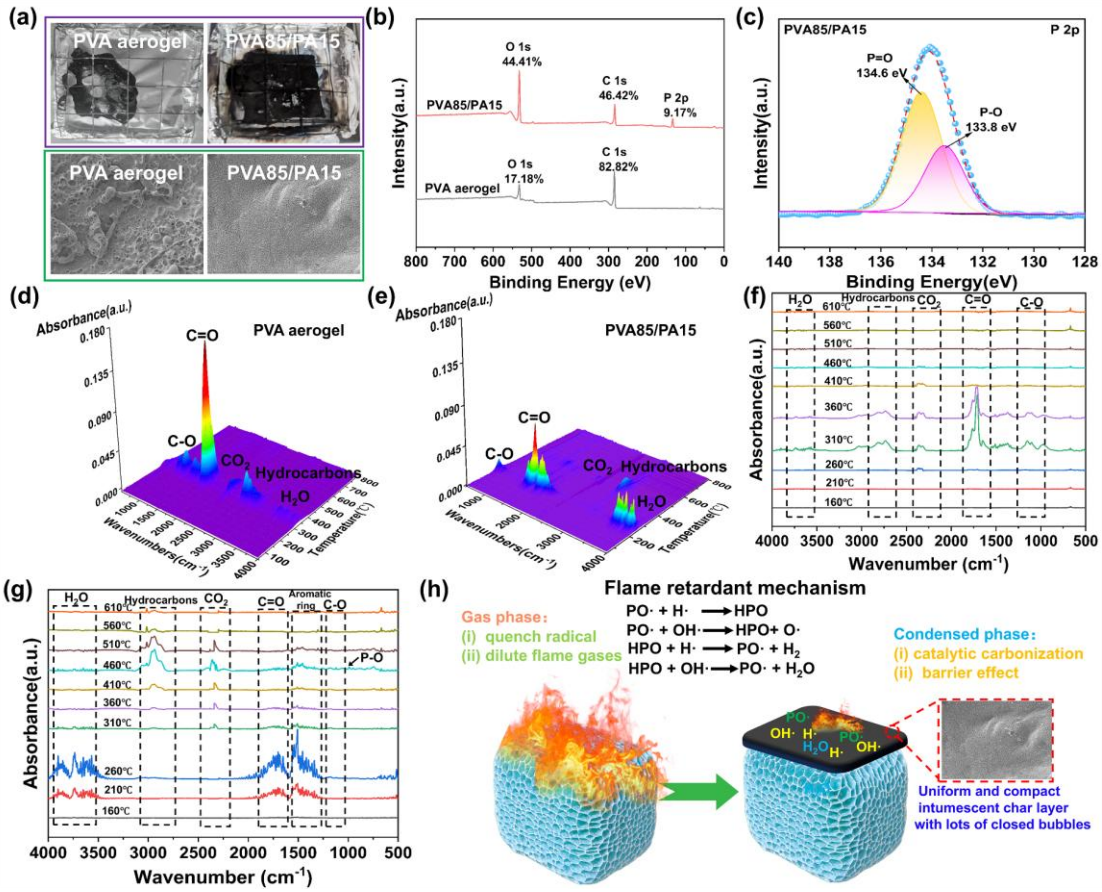

Figure 6. (a) Digital and SEM images of char residues for PVA aerogel and PVA85/PA15 composite aerogel. (b) XPS spectra of char residues for PVA aerogel and PVA85/PA15 composite aerogel. (c) High–resolution P2p spectra of char residue for PVA85/PA15 composite aerogel. 3D–TG–FTIR spectra depicting the pyrolysis products of (d) PVA aerogel and (e) PVA85/PA15 composite aerogel. Time-resolved

FTIR spectra illustrating the pyrolysis behavior of (f) PVA aerogel and (g) PVA85/PA15 composite aerogel. (h) Illustration of the flame retardancy mechanism in the PVA85/PA15 composite aerogel.

XPS result confirmed that the residual char from the PVA85/PA15 composite aerogel contained 9.17% of P (Fig.6b–c). Moreover, the atomic percentage of carbon dropped to 46.42%, whereas the atomic percentage of oxygen rose to 44.41%. The P 2p characteristic peaks of the PVA85/PA15 char, observed at binding energies of 134.6 and 133.8 eV, were assigned to P=O and P–O, respectively [61]. These results indicate the production of phosphoric acid or pyrophosphoric acid during the burning process. These phosphorus–based compounds played a critical role in the formation of a dense char layer, which in turn improved the fire–resistant performance of the composite aerogel.

The pyrolysis byproducts of aerogel samples were examined through TG–FTIR analysis (Fig.2d–g). For PVA aerogel, the absorption peak observed in the spectral region of 3700–3500 cm^{-1} was associated with the –OH stretching vibrations, indicating the occurrence of a dehydration process in PVA under thermal treatment. The presence of C–H and $–CH_2$ peaks at 3100-2700 cm^{-1} can be attributed to the thermal decomposition of PVA main chain. The absorption peak between 2400 to 2300 cm^{-1} was primarily due to CO_2 generated during the thermal degradation of PVA. Meanwhile, the C=O peak observed in the 1850-1700 cm^{-1} was attributed to random chain scission during PVA dehydration, leading to the formation of aldehydes and ketones. Additionally, a C–O absorption peak was also observed within 1250–1000

cm^{-1}, mainly originating from the release and subsequent transformation of hydrocarbons [43,62]. In contrast, the total pyrolysis products of PVA85/PA15 composite aerogel significantly reduced due to the incorporation of PA. Moreover, the release of water vapor showed significantly increased due to the catalytic effect of PA. The peak of aromatic compounds also presented within the range of 1850-1700 cm^{-1}, and a new P–O peak was observed in 1010 cm^{-1} [63,64]. These results revealed that the released of phosphorus–containing free radicals during the pyrolysis of the composite aerogel can effectively quench the active free radicals generated from PVA decomposition, thereby suppressing the combustion process.

According to the analysis, the PVA85/PA15 composite aerogel can be primarily attributed to two key flame–retardant mechanisms (Fig.6h). Initially, in the condensed phase, flame retardancy was achieved through the formation of a protective char layer, which acted as a barrier against heat and oxygen transfer. During the combustion process, PA first undergoes decomposition to generate highly reactive phosphoric acid and pyrophosphoric acid, serving as an ‘acid source’ that facilitate the dehydration and carbonization processes of PVA, which functions as the ‘carbon source’. PA alters the carbonization pathway of PVA, facilitating the conversion of volatile flammable gases into stable aromatic carbon structures, thus promoting the development of a protective char structure. This compact carbonaceous layer, which contains a lot of closed–cell bubbles, effectively inhibits the transfer of heat and oxygen and suppresses the release of PVA pyrolysis products. Secondly, in the gas phase, flame retardancy was achieved through dilution, heat absorption, and radical quenching. During thermal

decomposition, PVA also functions as a ‘gas source’, releasing a substantial amount of non–flammable water vapor. This vapor dilutes flammable gases and absorbs heat, thereby reducing fire intensity. Additionally, PA acts as a free radical scavenger, which quenches high–energy free radicals produced during PVA pyrolysis and thus interrupts the combustion chain reaction occurring in the gas phase. In summary, PA acts not only as an ‘acid source’ but also as a free radical scavenger, whereas PVA functions as both ‘carbon source’ and ‘gas source’. These two components form an intrinsic IFR system, which achieves flame retardancy through the cooperative action of both gas–phase and condensed–phase mechanisms.

3.6. Hydrophobic Treatment

To address the water sensitivity of PVA85/PA15 composite aerogel, PMHS was introduced via a simple CVD method to enhance its hydrophobicity. As shown in Fig. 7a, the original PVA85/PA15 aerogel showed a water contact angle (WCA) of only 36.2° at 0.1 s, and liquid droplets from various beverages rapidly penetrated its surface, indicating strong hydrophilicity. In contrast, PMHS–PVA85/PA15 composite aerogel exhibited significantly improved hydrophobic performance. Its WCA reached 145.6ºat 10 min, and droplets of various beverages remained stable on the surface without penetration or spreading. These results demonstrated that a highly hydrophobic PMHS–PVA85/PA15 composite aerogel was successfully prepared. In addition, the surface chemical composition of PMHS–PVA85/PA15 composite aerogel was analyzed using XPS, as shown in Fig. 7 b–d. Compared to the original PVA85/PA15 aerogel, PMHS–PVA85/PA15 composite aerogel exhibited the presence of Si element with an atomic

percentage of 1.73%. Meanwhile, the atomic percentage of C increased to 69.99% in the modified aerogel, while that of O significantly decreased to 26.69%. Furthermore, a new peak at 283.7 eV appeared in the C 1s spectrum, which may be due to C–Si bond. Meanwhile, the C 1s spectrum exhibited peaks at 286.1 eV, corresponding to the C–O bond, and at 284.8 eV, attributed to the C–C bond, with significantly reduced peak areas observed. Besides, the Si 2p peaks at 103.1 and 101.5 eV were attributed to Si–O and Si–C bonds, respectively. These findings revealed that a substantial number of low surface energy methyl ($–CH_3$) groups were successfully formed onto the surface of the modified aerogel [65,66]. Moreover, as shown in Table S4, PMHS–PVA85/PA15 composite aerogel exhibited only minor changes in certain performance, including bulk density, specific modulus, thermal conductivity, and flame retardancy, compared to the original PVA85/PA15 composite aerogel, indicating that the effects of hydrophobic modification can be negligible.

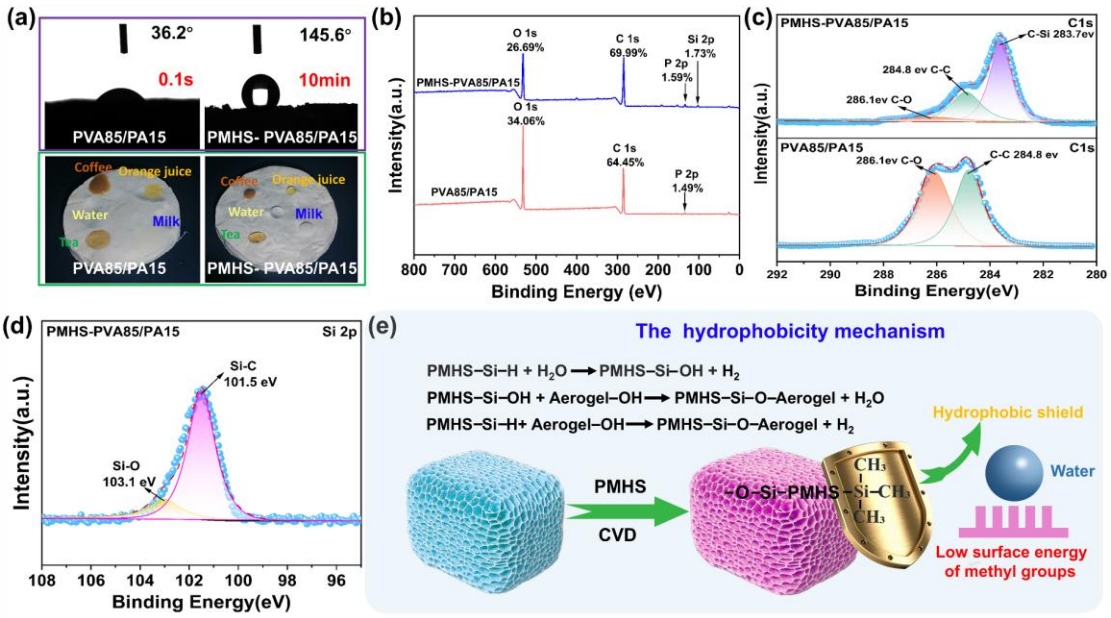

Fig.7. (a) WCA and various beverages droplets images on the surface of original PVA85/PA15 and PMHS–PVA85/PA15 composite aerogel. (b) XPS spectra of original

PVA85/PA15 and PMHS–PVA85/PA15 composite aerogel. (c)High-resolution C1s spectra of PVA85/PA15 and PMHS–PVA85/PA15 composite aerogel. (d)High–resolution Si2p spectra of PMHS–PVA85/PA15 composite aerogel. (e) Schematic diagram of hydrophobicity mechanism of PMHS–PVA85/PA15 composite aerogel.

In summary, PMHS vapor infiltrated the 3–D network structure of the PVA85/PA15 composite aerogel via the CVD method. A covalent reaction subsequently occurred between the Si–OH/Si–H groups in PMHS and –OH groups of the origin composite aerogel, leading to strong chemical anchoring. The original composite aerogel was predominantly covered with numerous low surface energy $–CH_3$ groups as hydrophobic shield (Fig.7e). This hydrophobic treatment approach not only effectively mitigated the inherent hydrophilicity of the original composite aerogel but also had minimal impact on its other properties. Therefore, the hydrophobic modification was served as an accurate, efficient, and technically feasible strategy, offering practical potential for real–world applications of the PMHS–PVA85/PA15 composite aerogel.

4. Conclusions

In this study, a green PVA–based composite aerogel with excellent overall performance was successfully fabricated. The aerogel demonstrates lightweight, high mechanical strength, superior thermal insulation, remarkable flame-retardant performance, and excellent hydrophobicity. The aerogel displayed a robust micro–nano 3–D network structure, attributed to enhanced interactions and advancements in the fabrication technique. Additionally, the intrinsically IFR system was forming in the

aerogel through utilizing bio–based PVA as the primary ‘carbon source’ and secondary ‘gas source’, while employing bio–based PA as the ‘acid source’. The resulting aerogel exhibited a considerably lower bulk density of 0.075 $g \cdot cm^{-3}$ and a markedly higher porosity of 94.21% compared to pure PVA aerogel. The compressive strength and specific modulus were notably enhanced by 225.7% and 294.5%, respectively. Moreover, the aerogel had a low thermal conductivity of 33.6 $mW \cdot m^{-1} \cdot K^{-1}$, exhibiting superior thermal insulation. With the introduction of PMHS via a CVD method, the surface of the modified aerogel exhibited numerous low surface energy $–CH_3$ groups, thereby conferring excellent hydrophobicity with a significantly increased WCA of 145.6º. This work delivers a green fabrication strategy for fully bio–based high–performance composite aerogels to address the energy crisis and advance sustainable development.

Acknowledgements

This work was financially supported by the National Key R&D Program of China (2022YFC3003105), Natural Science Foundation of China (grant nos. 52173069), and the Key Research and Development Projects in Heilongjiang Province (2024ZXDXA29).

References

[1] X. An, C. Ma, L. Gong, C. Liu, N. Li, Z. Liu, X. Li, Ionic-physical–chemical triple cross-linked all-biomass-based aerogel for thermal insulation applications, J. Colloid Interface Sci. 668 (2024) 678-690.https://doi.org/10.1016/j.jcis.2024.04.138

[2] X.C. Lin, S.L. Li, W.X. Li, Z.H. Wang, J.Y. Zhang, B.W. Liu, T. Fu, H.B. Zhao, Y. Z. Wang, Thermo-Responsive Self-Ceramifiable Robust Aerogel with Exceptional Strengthening and Thermal Insulating Performance at Ultrahigh Temperatures, Adv. Funct. Mater. 33(2023)2214913. https://doi.org/10.1002/adfm.202214913

[3] H. B. Chen, D.A. Schiraldi, Flammability of Polymer/Clay Aerogel Composites: An Overview, Polym. Rev. 59 (2019) 1-24.https://doi.org/10.1080/15583724.2018.1450756

[4] A. Di, C. Schiele, S. Hadi, L. Bergstrom, Thermally insulating and moisture-resilient foams based on upcycled aramid nanofibers and nanocellulose, Adv Mater. 2305195-2305204 (2023). https://doi.org/10.1002/adma.202305195

[5] Y. Xu, C. Yan, C. Du, K. Xu, Y. Li, M. Xu, S. Bourbigot, G. Fontaine, B. Li, L. Liu, High-strength, thermal-insulating, fire-safe bio-based organic lightweight aerogel based on 3D network construction of natural tubular fibers, Compos. Part B Eng. 261 (2023) 110809. https://doi.org/10.1016/j.compositesb.2023.110809

[6] H. B. Chen, E. Hollinger, Y. Z. Wang, D.A. Schiraldi, Facile fabrication of poly(vinyl alcohol) gels and derivative aerogels, Polymer. 55 (2014) 380-384. https://doi.org/10.1016/j.polymer.2013.07.078

[7] C. B. Ma, B. Du, E. Wang, Self-crosslink method for a straightforward synthesis of poly (vinyl alcohol)-based aerogel assisted by carbon nanotube, Adv. Funct. Mater. 27 (10) (2017). https://doi.org/10.1002/adfm.201604423

[8] Z. Bai, J. Jiang, H. Zhu, D. Zhang, H. Zhang, Y. Yu, F. Quan, Multi-network PVA/SA aerogel fiber: Unveiling superior mechanical, thermal in

sulation, and extreme condition stability, Polym. Degrad. Stab. 223 (2024) 1107 34. https://doi.org/10.1016/j.polymdegradstab.2024.110734

[9] J. Tu, T. Mao, S. Xie, H. Xiao, P. Wang, Lightweight, ultrahigh-strength and flame-retardant cellulose aerogel crosslinked with a reactive P/N-rich curdlan derivative, Int. J. Biol. Macromol.281(2024)135991. https://doi.org/10.10 16/j.ijbiomac.2024.135991

[10] Y. Shi, Y. Xu, K. Xu, C. T. Yan, A. Qin, C. L. Du, M. J. Xu, C. Wang, B. Li, L. B. Liu, Fire-resistant and thermal-insulating alginate aerogel with intelligent bionic armor for exceptional mechanical and fire early-warning performance, Chem. Eng. J. 498 (2024) 155181. https://doi.org/10.1016/j.cej.2024.155181

[11] C. L. Du, Y. Xu, C.T. Yan, W.J. Zhang, H.J. Hu, Y.Q. Chen, M.J. Xu, C. M. Wang, B. Li, L.B. Liu, Facile construction strategy for intrinsically fire-safe and thermal-insulating bio-based chitosan aerogel, Sustain. Mater. Technol. 39 (2024) e00794. https://doi.org/ 10.1016/j.susmat. 2023.e00794

[12] X. Wang, Y. Li, D. Meng, X. Gu, J. Sun, Y. Hu, S. Bourbigot, S. Zhang, A Review on Flame-Retardant Polyvinyl Alcohol: Additives and Technologies, Polymer Revs. 63 (2023) 324-364. https://doi.org/10.1080/15583724.2022.2076694

[13] S. L. Gao, R. P. Wang, Y. Xu, H. Zhang, S. Zhang, M. J. Xu, L. B. Liu, B. Tao, H. Xue, S. Li, B. Li, Facile construction of a micro-nano structure of green polyvinyl alcohol-based composite aerogel with superior mechanical properties, thermal insulation, and fire safety, Polym. Degrad. Stab.241 (2025) 111522.https://doi.org/10.1016/j.polymdegradstab.2025.111522

[14] Y. Zhou, W. He, J. Song, D. Xu, H. Wu, J. Guo, Flammability and thermal analysis of vertically oriented polyvinyl alcohol/DOPO derivative/MXene composite aerogel, Polym. Degrad. Stab. 229 (2024) 111006. https://doi.org/10.1016/j.polymdegradstab.2024.111006

[15] W. W. Guo, J. Liu, P. Zhang, L. Song, X. Wang, Y. Hu, Multi-functional hydroxyapatite/polyvinyl alcohol composite aerogels with self-cleaning, superior fire resistance and low thermal conductivity, Compos. Sci. Technol. 158 (2018) 128-136. https://doi.org/10.1016/j.compscitech.2018.01.02

[16] Y. T. Wang, S. F. Liao, K. Shang, M. J. Chen, J. Q. Huang, Y. Z. Wang, D.A.Schiraldi, Efficient Approach to Improving the Flame Retardancy of Poly (vinyl alcohol)/Clay Aerogels: Incorporating Piperazine-Modified Ammonium Polyphosphate, ACS Appl. Mater. 7 (2015) 1780-1786. https://doi.org/10.1021/am507409d

[17] H. B. Chen, Y. Z. Wang, D.A. Schiraldi, Preparation and Flammability of Poly (vinyl alcohol) Composite Aerogels, ACS Appl. Mater. Interfaces. 6 (2014) 6790-6796. https://doi.org/10.1021/am500583x

[18] Y. Luo, D. Xie, Y. Chen, T. Han, R. Chen, X. Sheng, Y. Mei, Synergistic effect of ammonium polyphosphate and α-zirconium phosphate in flame-retardant poly (vinyl alcohol) aerogels, Polym. Degrad. Stab. 170 (2019) 109019. https://doi.org/10.1016/j.polymdegradstab.2019.109019

[19] R.H.E.M. Koppelaar, H.P. Weikard, Assessing phosphate rock depletion and phosphorus recycling options, Global Environ Chang. 23 (2013) 1454-1466.

https://doi.org/10.1016/j.gloenvcha.2013.09.002

[20] T. C. Mokhena, E. R. Sadiku, S. S. Ray, M. J. Mochane, K. P. Matabola, M. Motloung, Flame retardancy efficacy of phytic acid: An overview, J. Appl. Polym. Sci. 139 (2022) e52495. https://doi.org/10.1002/app.52495

[21] K. Sykam, M. Försth, G. Sas, Á. Restás, O. Das, Phytic acid: A bio-based flame retardant for cotton and wool fabrics, Ind. Crops Prod.164 (2021) 113349.https://doi.org/10.1016/j.indcrop.2021.113349

[22] J. Jiang, W. Yang, S.H. Lee, W.C. Lum, G. Du, Y. Ren, X. Zhou, J. Zhang, Reactive bio-based flame retardant derived from chitosan, phytic acid, and epoxidized soybean oil for high-performance biodegradable foam, Int. J. Biol. Macromol. 307 (2025) 142137.https://doi.org/10.1016/j.ijbiomac.2025.142137

[23] M. Cao, B.W. Liu, L. Zhang, Z. C. Peng, Y.Y. Zhang, H. Wang, H.B. Zhao, Y. Z. Wang, Fully biomass-based aerogels with ultrahigh mechanical modulus, enhanced flame retardancy, and great thermal insulation applications, Compos. Part B Eng. 225 (2021) 109309.https://doi.org/10.1016/j.compositesb.2021.109309

[24] Y. T. Wang, H. B. Zhao, M. L. Guo, K. Degracia, H. Sun, M. Z. Sun, Z. Y. Zhao, D.A. Schiraldi, Y. Z. Wang, Rigid and Fire-Resistant All-Biomass Aerogels, ACS Sustainable Chem. Eng.10 (2022) 12117-12126. https://doi.org/10.1021/acssuschemeng.2c02109

[25] E. Liu, H. Nie, H. Zhang, Y. Chang, Y. Ren, Z. Chen, Z. Wu, Biomimetic aerogels of small intestinal villi guided by biobased electrolyte ligands: High flame retardation, heat insulation, antibacterial and degradation performance, Chem. Eng. J.504 (2025)

158665. https://doi.org/10.1016/j.cej.2024.158665

[26] H. Wang, M. Cao, H. B. Zhao, J. X. Liu, C. Z. Geng, Y. Z. Wang, Double-cross-linked aerogels towards ultrahigh mechanical properties and thermal insulation at extreme environment, Chem. Eng. J. 399 (2020) 125698. https://doi.org/10.1016/j.cej.2020.125698

[27] V.G. Krishnan, C.V.S. Rosely, A. Leuteritz, E.B. Gowd, High-Strength, Flexible, Hydrophobic, Sound-Absorbing, and Flame-Retardant Poly (vinyl alcohol)/ Polyelectrolyte Complex Aerogels, ACS Appl. Polym. Mater.4 (2022) 5113-5124. https://doi.org/10.1021/acsapm.2c00639

[28] Yue Xu, Haojie Hu, Bin Tao, Ru Yin, Lubin Liu, Bin Li. Safe and economical preparation of amino acid-derived bio-based triazine char-forming agent for efficient intumescent flame retardant polypropylene. Constr. Build. Mater. 484, (2025) 141876. https://doi.org/10.1016/j.conbuildmat.2025.141876

[29] Y.P. Handa, D.D. Klug, Heat capacity and glass transition behavior of amorphous ice, J. Phys. Chem.92 (1988) 3323-3325. https://doi.org/10.1021/j100323a005

[30] Z. Ma, D. Meng, Z. Zhang, Y. Wang, Synergistic effect of green phosphorus-containing bio-based material and two-dimensional layered material composite on flame-retardant property of polyvinyl alcohol, Thermochim. Acta. 707 (2022) 179118. https://doi.org/10.1016/j.tca.2021.179118

[31] C. Wang, Z. Zhang, Z. Ma, Z. Zhou, Y. Wang, Design of a bio-based flame retardant for polyvinyl alcohol with superior flame retardant, mechanical and UV-blocking properties, J. Polym. Res. 30 (2023) 228. https://doi.org/10.1007/s1096

5-023-03611-y

[32] G. Jiang, J. Qiao, F. Hong, Application of phosphoric acid and phytic acid-doped bacterial cellulose as novel proton-conducting membranes to PEMFC, Int. J. Hydrog. Energy. 37 (2012) 9182-9192. https://doi.org/10.1016/j.ijhydene.2012.02.195

[33] X.W. Cheng, J.P. Guan, X.H. Yang, R.C. Tang, Y. Fan, Phytic acid/silica organic-inorganic hybrid sol system: a novel and durable flame retardant approach for wool fabric, J MATER RES TECHNOL. 9 (2020) 700-708. https://doi.org/10.1016/j.jmrt.2019.11.011

[34] T. Zhou, X. Cheng, Y. Pan, C. Li, L. Gong, Mechanical performance and thermal stability of polyvinyl alcohol-cellulose aerogels by freeze drying, Cellulose. 26 (2019) 1747-1755. https://doi.org/10.1007/s10570-018-2179-3

[35] G. Olivieri, A. Cossaro, E. Capria, L. Benevoli, M. Coreno, M. De Simone, K.C. Prince, G. Kladnik, D. Cvetko, B. Fraboni, A. Morgante, L. Floreano, A. Fraleoni-Morgera, Intermolecular Hydrogen Bonding and Molecular Orbital Distortion in 4-Hydroxycyanobenzene Investigated by X-ray Spectroscopy, J. Phys. Chem. C. 119 (2015) 121-129.https://doi.org/10.1021/jp5100878

[36] A. Hill, F. Wang, Intramolecular O·H Hydrogen Bonding of Salicylic Acid: Further Insights from O 1s XPS and 1H NMR Spectra Using DFT Calculations, J. Phys. Chem. A. 127 (2023) 2705-2716.https://doi.org/10.1021/acs.jpca.2c08981

[37] A. Varamesh, Y. Zhu, G. Hu, H. Wang, H. Rezania, Y. Li, Q. Lu, X. Ren, F. Jiang, S. Bryant, J. Hu, Fully biobased thermal insulating aerogels with superior fire-retardant

and mechanical properties, Chem. Eng. J. (2024) 153587. https://doi.org/10.1016/j.cej.2024.153587

[38] L. Wang, M. Luo, Z. Zhang, D. Ji, X. Chang, Y. Zhu, Ultra-stretchable, robust, self-healable conductive hydrogels enabled by the synergistic effects of hydrogen bonds and ionic coordination bonds toward high-performance e-skins, Chem. Eng. J. 500 (2024) 156800. https://doi.org/10.1016/j.cej.2024.156800

[39] J. Lyu, Q. Zhou, H. Wang, Q. Xiao, Z. Qiang, X. Li, J. Wen, C. Ye, M. Zhu, Mechanically Strong, Freeze-Resistant, and Ionically Conductive Organohydrogels for Flexible Strain Sensors and Batteries, Adv.Sci. 10 (2023) 2206591. https://doi.org/10.1002/advs.202206591

[40] S. Brunauer, P.H. Emmett, E. Teller, Adsorption of Gases in Multimolecular Layers, J. Am. Chem. Soc. 60 (1938) 309-319. https://doi.org/10.1021/ja01269a023

[41] E.P. Barrett, L.G. Joyner, P.P. Halenda, The Determination of Pore Volume and Area Distributions in Porous Substances. I. Computations from Nitrogen Isotherms, J. Am. Chem. Soc.73 (1951) 373-380. https://doi.org/10.1021/ja01145a126

[42] Z. Yang, H. Li, G. Niu, J. Wang, D. Zhu, Poly(vinylalcohol)/chitosan-based high-strength, fire-retardant and smoke-suppressant composite aerogels incorporating aluminum species via freeze drying, Compos. Part B Eng. 219(2021)108919. https://doi.org/10.1016/j.compositesb.2021.108919

[43] X. Hong, Y. Zheng, Y. Shi, W. Zheng, F. Lin, L. Xiong, A facile strategy for constructing lightweight, fire safety and compression resistance poly(vinylalcohol) aerogels with highly-efficient expansible graphene oxide/layered double hydroxides

hybrid synergistic flame retardant, J. Colloid Interface Sci. 650 (2023) 686-700. https://doi.org/10.1016/j.jcis.2023.07.028

[44] S. Zhang, J. Feng, J. Feng, Y. Jiang, L. Li, Ultra-low shrinkage chitosan aerogels trussed with polyvinyl alcohol, Mater. Des. 156 (2018) 398-406. https://doi.org/10.1016/j.matdes.2018.07.004

[45] Q. Cen, S. Chen, D. Yang, D. Zheng, X. Qiu, Full Bio-Based Aerogel Incorporating Lignin for Excellent Flame Retardancy, Mechanical Resistance, and Thermal Insulation, ACS Sustainable Chem. Eng.11 (2023) 4473-4484. https://doi.org/10.1021/acssuschemeng.2c07652

[46] J. Xu, X. Ao, J. de la Vega, F. Guo, Z. Xie, F. Liang, D.-Y. Wang, J. Wu, Poly(vinyl alcohol) Composite Aerogel toward Lightweight, Remarkable Flame Retardancy, and Thermal Insulation Properties by Incorporating Carbon Nanohorns and Phytic Acid, ACS Appl. Polym. Mater., 6 (2024) 8027-8039. https://doi.org/10.1021/acsapm.4c00729

[47] T. Deng, H. Li, Y. Li, C. Jiang, Y. He, T. Yang, L. Zhu, L. Xie, Environment friendly biomass composite aerogel with reinforced mechanical properties for thermal insulation and flame retardancy application, Polym. Eng. Sci., 63 (2023) 4084-4097. https://doi.org/10.1002/pen.26509

[48] X. Long, P. Tang, L. Zhou, W. Chen, S. Ren, Y. Qiu, L. Sui, X. Wei, J. Liao, Reversible sacrificial hydrogen bonds enhanced ultra-high strength polybenzoxazine aerogel for thermal insulation, Appl. Surf. Sci. 613 (2022) 156004. https://doi.org/10.1016/j.apsusc.2022.156004

[49] X. Wang, Z. Li, M. Hu, Q. Liu, M. Li, X. Cheng, X. Wu, Engineering binary-network structured montmorillonite/silica composite aerogels with improved mechanical strength as water-resistant thermal insulators, Appl. Clay Sci. 251 (2024) 107316. https://doi.org/10.1016/j.clay.2024.107316

[50] A.-H. Kang, K. Shang, D.-D. Ye, Y.-T. Wang, H. Wang, Z.-M. Zhu, W. Liao, S. Xu, Y.-Z. Wang, D.A. Schiraldi, Rejuvenated fly ash in poly(vinyl alcohol)-based composite aerogels with high fire safety and smoke suppression, Chem. Eng. J. 327 (2017) 992-999, http://dx.doi.org/10.1016/j.cej.2017.06.158

[51] J. Yang, K.-Y. Chan, H. Venkatesan, E. Kim, M.H. Adegun, J.-H. Lee, X. Shen, J. K. Kim, Superinsulating BNNS/PVA Composite Aerogels with High Solar Reflectance for Energy-Efficient Buildings, Nano-Micro Lett. 14 (2022) 54. https://doi.org/10.1007/s40820-022-00797-6

[52] J. Zhu, F. Zhao, R. Xiong, T. Peng, Y. Ma, J. Hu, L. Xie, C. Jiang, Thermal insulation and flame retardancy of attapulgite reinforced gelatin-based composite aerogel with enhanced strength properties, COMPOS PART A-APPL S. 138 (2020) 106040. https://doi.org/10.1016/j.compositesa.2020.106040

[53] Q. Peng, Y. Qin, X. Zhao, X. Sun, Q. Chen, F. Xu, Z. Lin, Y. Yuan, Y. Li, J. Li, W. Yin, C. Gao, F. Zhang, X. He, Y. Li, Superlight, Mechanically Flexible, Thermally Superinsulating, and Antifrosting Anisotropic Nanocomposite Foam Based on Hierarchical Graphene Oxide Assembly, ACS Appl. Mater. Interfaces. 9 (2017) 44010-44017. https://doi.org/10.1021/acsami.7b14604

[54] S. Xiang, C. Chen, F. Liu, L. Wang, J. Feng, X. Lin, H. Yang, X. Feng, C. Wan,

Phosphorus and nitrogen supramolecule for fabricating flame-retardant, transparent and robust polyvinyl alcohol film, J. Colloid Interface Sci. 669(2024)775-786. https://doi.org/10.1016/j.jcis.2024.05.060

[55] Z. Yang, D. Zhu, Synthesis and characterization of AlCl3-chitosan composite aerogels incorporating polyvinyl alcohol and bentonite clay, J. Sol-Gel Sci. Technol., 103 (2022) 722-729.https://doi.org/10.1007/s10971-022-05848-3

[56] N. Wu, F. Niu, W. Lang, M. Xia, Highly efficient flame-retardant and low-smoke-toxicity poly(vinyl alcohol)/alginate/ montmorillonite composite aerogels by two-step crosslinking strategy, Carbohydr. Polym., 221 (2019) 221-230. https://doi.org/10.1016/j.carbpol.2019.06.007

[57] Y. T. Wang, H. B. Zhao, K. Degracia, L. X. Han, H. Sun, M. Sun, Y. Z. Wang, D.A. Schiraldi, Green Approach to Improving the Strength and Flame Retardancy of Poly(vinyl alcohol)/Clay Aerogels: Incorporating Biobased Gelatin, ACS Appl. Mater. Interfaces, 9 (2017) 42258-42265. https://doi.org/10.1021/acsami.7b14958

[58] H. Jin, X. Zhou, T. Xu, C. Dai, Y. Gu, S. Yun, T. Hu, G. Guan, J. Chen, Ultralight and Hydrophobic Palygorskite-based Aerogels with Prominent Thermal Insulation and Flame Retardancy, ACS Appl. Mater. Interfaces.12 (2020) 11815-11824.https://dx.doi.org/10.1021/acsami.9b20923

[59] Y. Dong, Z. Gui, Y. Hu, Y. Wu, S. Jiang, The influence of titanate nanotube on the improved thermal properties and the smoke suppression in poly(methyl methacrylate), J. Hazard. Mater. 209-210 (2012) 34-39. https://doi.org/10.1016/j.jhazmat.2011.12.048

[60] L. Zhao, C. Zhao, C. Guo, Y. Li, S. Li, L. Sun, H. Li, D. Xiang, Polybenzoxazine

Resins wit Microspheres: Synthesis, Flame Retardancy, Mechanisms, and Applications, ACS Omega. 4 (2019) 20275-20284. https://doi.org/10.1021/acsomega.9b02752

[61] M. Li, Z. Zhu, Y. Chen, Y. Pan, X. Cao, Y. Jing, R. Jiao, H. Sun, J. Li, A. Li, Preparation of composite aerogels with excellent flame retardant and thermal insulation properties based on modified hollow glass microspheres, Polym. Degrad. Stab.228 (2024) 110898. https://doi.org/10.1016/j.polymdegradstab.2024.110898

[62] W. Cai, J. Wang, Y. Pan, W. Guo, X. Mu, X. Feng, B. Yuan, X. Wang, Y. Hu, Mussel-inspired functionalization of electrochemically exfoliated graphene: Based on self-polymerization of dopamine and its suppression effect on the fire hazards and smoke toxicity of thermoplastic polyurethane, J. Hazard. Mater. 352 (2018) 57-69. https://doi.org/10.1016/j.jhazmat.2018.03.021

[63] C. Ma, J. Li, Synthesis of an organophosphorus flame retardant derived from daidzein and its application in epoxy resin, COMPOS PART B-ENG. 178 (2019) 107471. https://doi.org/10.1016/j.compositesb.2019.107471

[64] H. Cui, N. Wu, X. Ma, F. Niu, Superior intrinsic flame-retardant phosphorylated chitosan aerogel as fully sustainable thermal insulation bio-based material, Polym. Degrad. Stab. 207 (2023) 110213. https://doi.org/10.1016/j.polymdegradstab.2022.110213

[65] Q. Zhang, X. Wang, X. Tao, Z. Li, X. Li, Z. Zhang, Polyvinyl alcohol composite aerogel with remarkable flame retardancy, chemical durability and self-cleaning property, Compos. Commun. 15 (2019) 96-102. https://doi.org/10.1016/j.coco.2019.07.003

[66] A. Walkiewicz-Pietrzykowska, K. Jankowski, J. Kurjata, R. Dolot, R. Brzozowski, J. Zakrzewska, P. Uznanski, Silicon Oxycarbide Thin Films Produced by Hydrogen-Induced CVD Process from Cyclic Dioxa-Tetrasilacyclohexane, Materials.18 (2025). https://doi.org/10.3390/ma18122911